Response surface methodology box-behnken design to optimise the hydrothermal synthesis of gadolinium nanoparticles

Wyantuti, Santhy; Fadhilatunnisa, Balqis; Fauzia, Retna Putri; Jia, Qi; Rahmani, Azmi Aulia; Irkham; Bahti, Husein Hernadi

Important note
To cite this publication, please use the final published version (if applicable).
Please check the document version above.

Contents lists available at ScienceDirect

Chinese Journal of Analytical Chemistry

Response surface methodology box-behnken design to optimise the hydrothermal synthesis of gadolinium nanoparticles

Santhy Wyantuti [a,*], Balqis Fadhilatunnisa [a], Retna Putri Fauzia [a,b], Qi Jia [c], Azmi Aulia Rahmani [a], Irkham [a], Husein Hernadi Bahti [a,b]

[a] Department of Chemistry, Faculty of Mathematics and Natural Sciences, Universitas Padjadjaran, Jl. Raya Bandung-Sumedang Km. 21 Jatinangor, Sumedang 45363, Indonesia
[b] Central Laboratory, Universitas Padjadjaran, Jl. Raya Bandung-Sumedang Km. 21 Jatinangor, Sumedang 45363, Indonesia
[c] Department of Biotechnology, Faculty of Applied Sciences, Delft University of Technology, Van der Maasweg 9, 2629 HZ, Delft, the Netherlands

ARTICLE INFO

ABSTRACT

Gadolinium (Gd) nanoparticles (NPs) are increasingly considered as a viable alternative to clinically employed Gd chelates in magnetic resonance imaging (MRI). The utilisation of these materials as contrast agents offers several advantages including lower toxicity, prolonged circulation time, and a sufficiently high Gd content, thereby enhancing disease imaging during MRI diagnosis. Therefore, this study synthesised Gd NPs using the hydrothermal method based on the response surface methodology Box-Behnken design (RSM-BBD) to determine the optimal conditions. In this experimental design, three independent variables, the mass of Gd_2O_3 (g), the synthesis temperature (°C) and time (h), were optimised to obtain sufficiently sized nanoparticles for further biomedical applications. In addition, polyethene glycol-6000 (PEG-6000) was used as a stabiliser to form uniformly sized nanoparticles. The optimal conditions were 0.4910 g of Gd_2O_3, a temperature of 180 °C, and a synthesis time of 7 h. Characterisation by scanning electron microscope-energy dispersive X-ray (SEM-EDX) and transmission electron microscope (TEM) demonstrated that the Gd NPs were spherical with a size range below 20 nm. Fourier transform infrared (FTIR) spectroscopy identified PEG molecules with low intensity on the Gd NPs and the obtained zeta potential value was +36.7±0.802 mV. The RSM-BBD analysis applied in this study facilitated the determination of the optimal synthesis conditions.

1. Introduction

Gadolinium (Gd) is a rare earth element (REE) that has garnered significant attention in recent years due to its fundamental importance and wide-ranging technological applications. Furthermore, its paramagnetic properties and excellent chemical stability have made Gd a subject of great interest in various fields [1]. Gd^{3+} ions with seven unpaired electrons in the 4f shell exhibit the largest magnetic moment amongst all elements (s=7/2) [2]. This unique characteristic often leads to the exhibition of high longitudinal relaxivity for water protons, making the element a valuable positive contrast agent in magnetic resonance imaging (MRI) [2,3].

Gd-based materials have long been applied as MRI contrast agents in clinical practice. Several Gd chelates have also been approved by the Food and Drug Administration (FDA) including macrocyclic products, such as Dotarem®, Gadavist®, and ProHance®, as well as linear products namely Magnevist®, Omniscan®, OptiMARK®, MultiHance®, and Eovist®. However, these Gd-based agents have several limitations,

including their potential toxicity and long-term *in vivo* deposition [4]. The toxicity can be attributed to the dissociation of Gd^{3+} from the chelate complexes. Free Gd^{3+} is a toxic heavy metal with a similar size to Ca^{2+} leading to competitive inhibition of Ca^{2+}-dependant biological processes. Several studies have shown that Gd^{3+} is deposited in other tissues including the skin, kidneys, liver, and brain. This unchelated metal retained in various tissues has the potential to become a source of toxicity [5,6].

Therefore, alternative strategies have been employed utilising nanoparticles that can passively target tumors through the enhanced permeability and retention (EPR) effect [2], eliminating the need for exogenous targeting ligands (e.g., folic acid) [7].

Nanoparticles ranging in size from 1 to 100 nm possess unique physical, chemical, and biological properties compared to larger-sized variants [8,9]. The relatively larger surface area to volume ratio, enhanced reactivity or stability, increased mechanical strength, and other properties make nanoparticles valuable in various applications [10]. Gd NPs exhibit higher binding strength compared to Gd complexes, making

them a promising alternative for Gd-based contrast agents due to stability, lower toxicity, longer retention time, and improved imaging capabilities [11].

Gd NPs can be made biocompatible for biomedical applications by coating them with a biocompatible shell, such as polyethene glycol (PEG). PEG is an attractive polymer for coating nanoparticles due to its $HO–(CH_2CH_2–O)_n–H$ structure. Furthermore, it is hydrophilic, non-toxic, and non-immunogenic, thereby protecting particles from protein adsorption and evading recognition by macrophages as foreign bodies, facilitating their uptake into cancer cells [12]. The use of PEG can also lead to uniform spherical particles, reduce aggregation, and decrease particle size [13].

Various methods have been successfully utilised to synthesise Gd NPs including thermal decomposition [14], pulsed laser ablation in a liquid (PLAL) [15], as well as polyol [11], solvothermal [13] and hydrothermal methods [16]. In this study, the hydrothermal method was combined with response surface methodology (RSM).

RSM is a suitable optimisation process that predicts the optimal parameters by modelling and analysing the influence of independent variables on the response [17]. The RSM Box-Behnken design (RSM-BBD) was selected due to its efficiency and fewer experimental unit requirements compared to other RSM methods [18]. This design involves three levels for each factor, thus requiring fewer experiments to evaluate multiple variables and their interactions [19]. This study aimed to synthesise Gd NPs using the hydrothermal method based on the BBD to achieve optimal experimental conditions.

The samples produced were characterised by scanning electron microscope-energy dispersive X-ray spectroscopy (SEM-EDX), transmission electron microscope (TEM) and high-resolution TEM (HRTEM), X-rays diffraction (XRD), Fourier transform infrared spectroscopy (FTIR), and zeta potential analysis. The anticipated Gd NPs were expected to be spherical, with a size below 100 nm, making them suitable candidates for further application as MRI contrast agents.

2. Experimental

2.1. Materials

The materials used were demineralised water, nitric acid (HNO_3, 65%, Merck), acetone (Sigma Aldrich), PEG 6000 (PEG-6000, Sigma Aldrich), and gadolinium oxide (Gd_2O_3 99.9%, Sigma Aldrich).

2.2. Equipment

The equipment consisted of laboratory glassware available in the Department of Chemistry. Other supporting equipment included a hydrothermal autoclave, an oven (Heraeus), a centrifuge (Beckman), a magnetic stirrer with heating (Falc F60), a particle size analyzer (PSA, Beckman Coulter), an SEM-EDX (Hitachi TM-3000), an FTIR, (PerkinElmer), a TEM (JEOL JEM-2100), (FE TEM, FEI Tecnai G2), XRD and a Zetasizer NanoZS (Malvern). Furthermore, computations were performed using the Minitab 18 software.

2.3. Experimental design

The RSM Box-Behnken experimental design utilised three independent variables including the mass of Gd_2O_3 (g), synthesis temperature (°C), and synthesis time (h) (Tables 1 and 2). The response variable was the smallest particle size.

2.4. Preparation of Gd_2O_3 solution

Gd_2O_3 solid namely 0.3263 g (low), 0.4894 g (medium), and 0.6525 g (high) was placed in a 50 mL glass container and 65% HNO_3 was added dropwise until it dissolved. Then, 20 mL of demineralised water was added and stirred using a magnetic stirrer on a hot plate until complete

Table 1
The independent factors for the synthesis of Gd NPs.

Factor	Name	Level		
		Low (−1)	Medium (0)	High (+1)
X_1	Gd_2O_3 Mass (g)	0.3263	0.4894	0.6525
X_2	Synthesis temperature (°C)	180	190	200
X_3	Synthesis time (h)	5	6	7

Table 2
Experimental design to determine the optimal synthesis conditions.

Run Order	X_1: Gd_2O_3 Mass (g)	X_2: Synthesis temperature (°C)	X_3: Synthesis time (h)
1	0.3263	180	6
2	0.6525	180	6
3	0.3263	200	6
4	0.6525	200	6
5	0.3263	190	5
6	0.6525	190	5
7	0.3263	190	7
8	0.6525	190	7
9	0.4894	180	5
10	0.4894	200	5
11	0.4894	180	7
12	0.4894	200	7
13	0.4894	190	6
14	0.4894	190	6
15	0.4894	190	6

dissolution. This process produced 0.9 mmol, 1.35 mmol, and 1.8 mmol Gd_2O_3 solutions.

2.5. Preparation of PEG-6000

PEG-6000 solid (10 g, 15 g, and 20 g) was placed in a 50 mL glass container and heated on a hot plate until the solid completely melted.

2.6. Preparation of Gd_2O_3 and PEG-6000 solutions

The 0.9, 1.35, and 1.8 mmol Gd_2O_3 solutions were added to the melted 10 g, 15 g, and 20 g PEG-6000 solutions, respectively and stirred using a magnetic stirrer on a hot plate until complete dissolution was achieved.

2.7. Synthesis of Gd NPs

The Gd_2O_3/PEG-6000 solutions were transferred into a Teflon autoclave at room temperature and then placed in an oven and heated at various temperatures and synthesis times as shown in Table 1 based on the experimental design created in Table 2. Subsequently, the solutions were cooled to room temperature, centrifuged at 10,000 rpm for 20 min and washed several times with acetone. The precipitate obtained was then dried in an oven at 60 °C for 24 h.

2.8. Optimisation of Gd NPs synthesis conditions

The Gd NPs produced were characterised using a PSA instrument. The smallest size obtained was used as the response variable, and analysis and optimization were conducted to determine the smallest response value using the RSM-BBD method in Minitab 18 software.

2.9. Characterisation of the Gd NPs

The synthesised Gd NPs were characterised using SEM-EDX, TEM, FTIR, and zeta potential instruments.
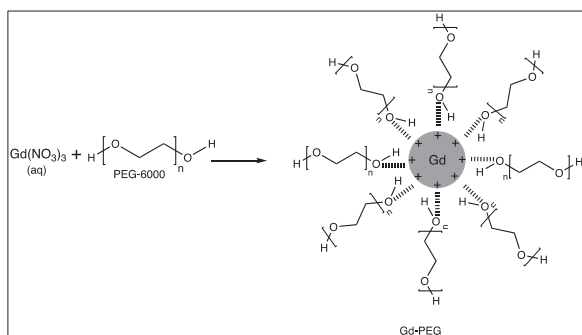
Fig. 1. Schematic illustration of the Gd-PEG interaction.

3. Results and discussion

3.1. Synthesis of Gd NPs using the hydrothermal method

The Gd NPs were synthesised using the hydrothermal method, employing a stainless-steel autoclave reactor with a polytetrafluoroethylene (PTFE) or Teflon inner chamber. The process was conducted under the high temperature and pressure generated within the closed vessel. Hydrothermal synthesis involves direct crystallization from the solution and comprises two steps, namely nucleation and crystal growth. Nucleation occurs in a saturated solution, with the dissolved substance precipitating into crystal clusters which grow concurrently through a series of processes involving the merging of these crystal growth units. $Gd(NO_3)_3$ is formed due to the addition of a small amount of HNO_3, as shown in Eq. (1). Subsequently, $Gd(NO_3)_3$ is ionised providing a source of Gd^{3+} for the formation of Gd NPs, as shown in Eq. (2).

$$Gd_2O_3 + 6HNO_3 \rightarrow 2Gd(NO_3)_3 + 3H_2O \qquad (1)$$

$$2Gd(NO_3)_3 \rightarrow 2Gd^{3+} + 6NO^{3-} \qquad (2)$$
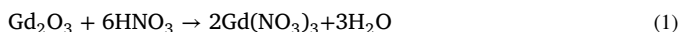
In the initial stage of hydrothermal synthesis, the Gd^{3+} precursor species are nucleated forming small clusters or nuclei, which continue to grow as the Gd^{3+} precursor diffuses within the solution, leading to the formation of Gd NPs.

The use of PEG-6000 as a stabilising agent was expected to provide a uniform spherical shape and reduce the size of nanoparticles by limiting the growth and aggregation between particles. As shown in Fig. 1, the hydroxyl groups of PEG cover the Gd^{3+} surface. The colloidal stability of Gd-PEG occurs due to the van der Waals forces between oxygen (negatively charged groups) on the PEG molecules and the positively charged groups on the Gd^{3+} surface. When PEG is adsorbed on the particle surface, the activity decreases, thereby limiting the particle growth rate.

The presence of PEG on the nanoparticle surface controls colloidal stability through steric repulsion, as indicated by an increase in molecular weight. This is because the distance between two nanoparticles increased with the elongation of the PEG chain, thereby increasing steric repulsion and preventing nanoparticle aggregation [20].

The selection of the independent variables or factors assumed to influence the synthesis was based on the study by Dougherty et al. (2019) [13], who used gadolinium acetate hydrate $(Gd(CH_3CO_2)_3 \cdot xH_2O)$ as the precursor (3.6 mmol) with 40 g of PEG-1000, synthesis temperature of 180 °C, and varying synthesis times of 3, 5, and 8 h.

3.2. Determination of the optimal gd NPs synthesis conditions

The experimental conditions and the smallest particle size of Gd NPs obtained are presented in Table 3. The smallest size obtained was 40 nm and the optimal synthesis conditions obtained in the 13th run were 0.4894 g of Gd_2O_3 at a temperature of 190 °C for 6 h.

Table 3
Gd NPs synthesis experimental data.

Run Order	Gd_2O_3 Mass (g)	Synthesis temperature (°C)	Synthesis time (h)	Smallest Size (nm)
1	0.3263	180	6	311
2	0.6525	180	6	284
3	0.3263	200	6	375
4	0.6525	200	6	258
5	0.3263	190	5	342
6	0.6525	190	5	311
7	0.3263	190	7	342
8	0.6525	190	7	311
9	0.4894	180	5	235
10	0.4894	200	5	134
11	0.4894	180	7	44
12	0.4894	200	7	48
13	0.4894	190	6	40
14	0.4894	190	6	258
15	0.4894	190	6	44

3.3. Regression model

The second-order polynomial regression model was applied to determine the relationship between the independent variables and the response variable, the smallest size of Gd NPs (Y):

$$Y = 0.1140 - 0.0258X_1 - 0.0074X_2 - 0.0346X_3 + 0.2021X_1{}^2 - 0.0091X_2{}^2 + 0.0104X_3{}^2 + 0.0225X_1X_2 - 0.0000\ X_1\ X_3 + 0.00262\ X_2X_3 \qquad (3)$$

where, X_1 is Gd_2O_3 mass (g), X_2 is the synthesis temperature (°C) and X_3 is the synthesis Time (h).

The coefficients of the regression Eq. (3) with positive signs indicated a positive influence, while coefficients with negative signs indicated a negative influence. Analysis of the regression coefficients showed that the mass of Gd_2O_3, temperature, and synthesis time had a negative relationship with the smallest size of Gd NPs.

3.4. Model suitability test

The model suitability test used the lack of fit test and the coefficient of determination (R^2) test. The lack of fit assessed the adequacy of the linear model, where the lack of significance indicated that the model was appropriate. To show the absence of a lack of fit in the model, the p-value must reject H_0. The p-value from the test was 0.844, which was greater than α (0.05). Therefore, there was no lack of fit, indicating the suitability of the generated second-degree polynomial model.

3.5. Residual assumption test

Residuals refer to the differences between the observed response values and the predicted values from the regression equation. The normal probability plot was used to test the assumption that the residuals were normally distributed, as shown in Fig. 2. The Anderson-Darling test ob-
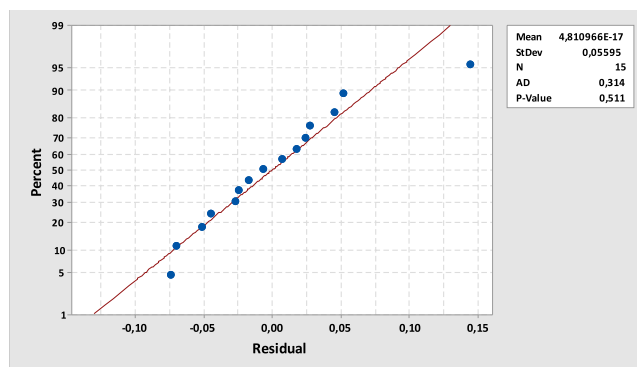

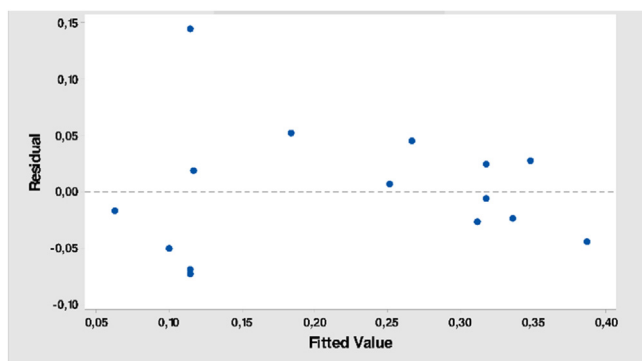**Fig. 2.** Normal probability plot of the residuals.

Fig. 3. Residual versus fitted value plot.

tained a *p*-value of 0.511 (*p*-value > 0.05), indicating that the assumption of a normal distribution had been met.

A residual versus fit plot was also used to prove that the residuals were randomly distributed and had a constant variance from one observation to another (homoscedasticity). The graph plotted the residuals on the *y*-axis and the fitted values on the *x*-axis. Based on Fig. 3, the data points did not exhibit any recognisable patterns, indicating that the residuals were distributed randomly and there was no heteroscedasticity in the regression model used.

3.6. Response surface plot

The response surface plots, such as contour and surface plots, were used to understand the relationship between the independent variables and the response variable, as well as to determine the desired response values and process conditions [21]. In the contour plots, the response surface was viewed as a two-dimensional (2D) plane, where all points with the same response were connected to create contour lines. Meanwhile, surface plots generally presented three-dimensional (3D) views to provide a clearer representation of the response [22].

In Fig. 4a, the smallest particle size with a response value < 0.10 µm was located in the lightest green area and was achieved by using a synthetic temperature of 200 °C and a mass of Gd_2O_3 at approximately 0.4894 g while keeping synthesis time constant at 6 h. In Fig. 4b, the smallest particle size with a response value < 0.10 µm was in the dark blue area and was achieved with a synthesis time ranging from 6.5 to 7 h and a mass of Gd_2O_3 of approximately 0.4894 g while keeping the synthesis temperature constant at 190 °C. Fig. 4c shows the smallest particle size with a response value < 0.08 µm in the dark blue area was achieved by using a synthesis time ranging from 6.5 to 7 h and a temperature ranging from 180 to 185 °C while keeping the mass of Gd_2O_3 constant at 0.4894g.

Based on surface plots in Fig. 5a, a reduction in particle size occurred with 0.4894 g of Gd_2O_3 and a decrease in temperature to 180 °C. A reduction in particle size occurred with 0.5 g of Gd_2O_3 and an increase in synthesis time to 7 h (Fig. 5b), as well as a decrease in temperature and an increase in synthesis time to 180 °C for 7 h (Fig. 5c).

3.7. Optimal conditions for Gd NPs synthesis

The optimum conditions for Gd NPs synthesis were expected to achieve the smallest particle size or reduce the response value.

Based on Fig. 6, the optimum conditions for Gd NPs synthesis were 0.4910 g Gd_2O_3 at a temperature of 180 °C for 7 h, leading to Gd NPs with the smallest size of 0.06 µm. However, these predicted values must be confirmed experimentally to determine both the size and shape.

With a larger mass of Gd_2O_3 as the source of Gd^{3+}, the diffusion rate increased, leading to larger particle sizes. When there was more Gd^{3+}, there were sufficient Gd^{3+} precursors for nucleus growth, causing larger sizes. However, other factors, such as synthesis time and temperature,
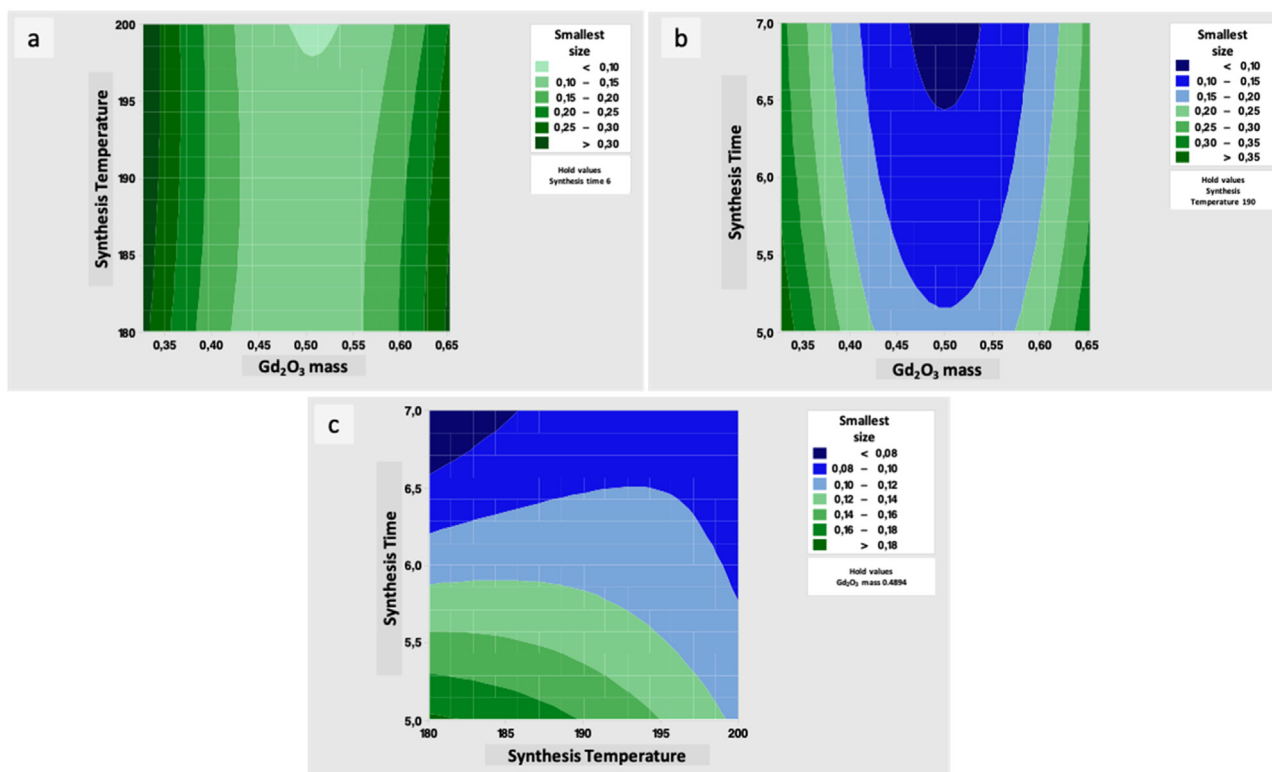

Fig. 4. Contour plot of factors X_1 and X_2 against the response (a), contour plot of factors X_1 and X_3 against the response (b), and contour plot of factors X_2 and X_3 against the response (c).
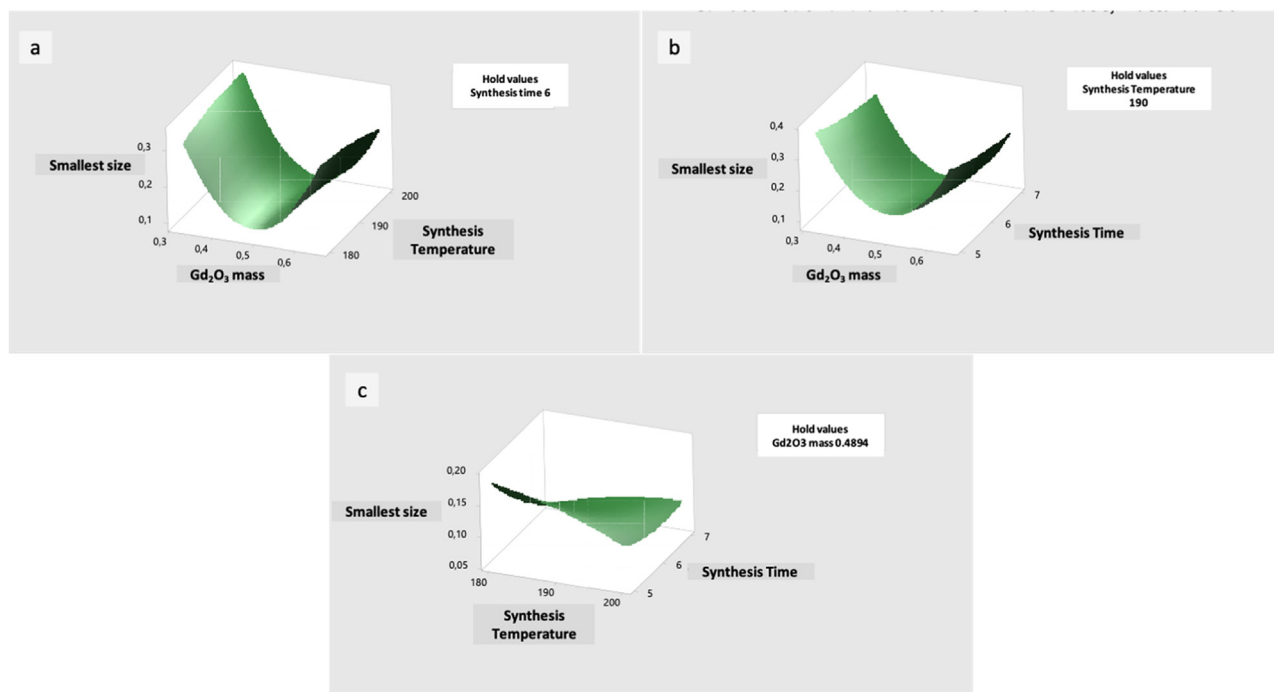
Fig. 5. Surface plot of factors X_1 and X_2 against the response (a), surface plot of factors X_1 and X_3 against the response (b), and surface plot of factors X_2 and X_3 against the response (c).
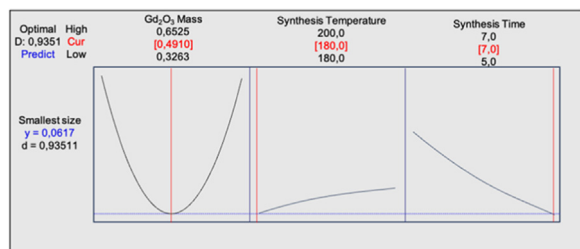

Fig. 6. Response optimisation.

were involved, leading to the optimum conditions of using a moderate level of Gd_2O_3.

Synthesis time affected the nucleation rate and the number of nuclei formed. A prolonged synthesis allowed more time for nucleation to occur, leading to more nuclei and smaller nanoparticles. During nucleation, there was a high consumption of Gd^{3+} precursor, which limited the growth due to a deficiency of diffusing Gd^{3+} causing smaller-sized nanoparticles.

Synthesis temperature was related to kinetic energy, where higher temperatures created higher kinetic energy. This affected the movement of particles, leading to increased collisions and agglomeration or the formation of larger groups of nanoparticles.

3.8. Characterisation of Gd NPs created using the optimal synthesis conditions

The Gd NPs synthesised under the optimum conditions of 0.4910 g of Gd_2O_3 at 180 °C for 7 h were characterised by SEM-EDX to determine the morphology and size, as shown in Fig. 7.

The SEM micrographs in Fig. 7 showed that the Gd NPs were spherical but not fully uniform as there was some agglomeration due to some relatively large spherical particles. According to Ref. [10], this agglomeration could be attributed to the use of high molecular weight PEG. Long PEG chains contain numerous hydrogen bonds that induce inter-
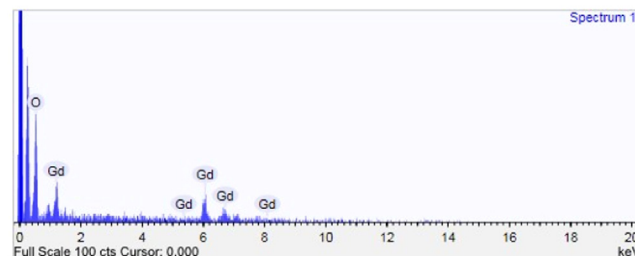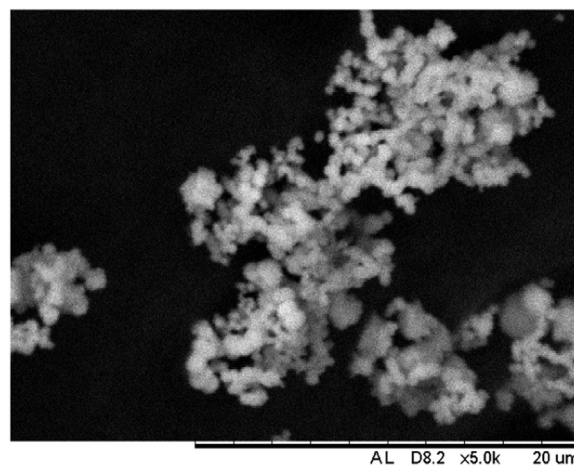

Fig. 7. SEM characterisation of Gd NPs at 5000x magnification and their EDX spectrum.

actions, leading to agglomeration. The spherical nanoparticles ranged in size from 46.9 to 141 nm, indicating that Gd NPs 40−60 nm in size were formed.

The SEM was equipped with EDX to identify the sample's elemental composition. The EDX spectrum in Fig. 7 displayed characteristic
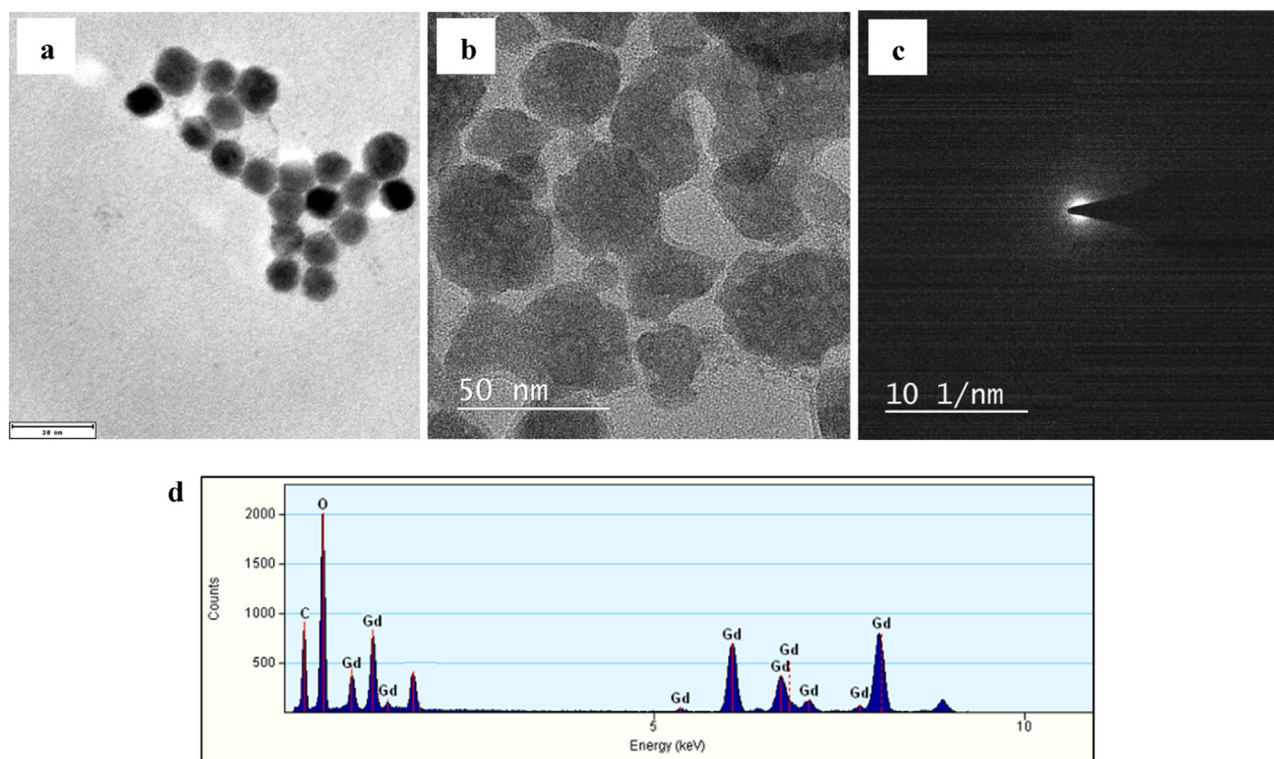
Fig. 8. TEM (a) and HRTEM (b) morphologies of Gd NPs. Selected area electron diffraction (SAED) and its EDX-spectrum are also included (c and d).
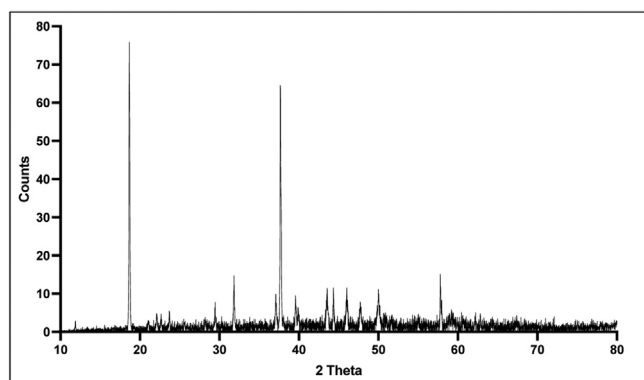

Fig. 9. X-ray diffraction (XRD) spectra of Gd NPs.

Fig. 10. FTIR Spectrum of PEG-6000 (a) and Gd NPs (b).

peaks for Gd and Oxygen (O) atoms, confirming that the nanoparticles contained Gd and Oxygen, with weight percentages of 56.077% and 43.923% and atomic percentages of 11.496% and 88.504%, respectively.

TEM and HRTEM confirmed the spherical morphology of the Gd NPs with particles smaller than 20 nm under the optimal synthesis conditions, leading to an average smallest particle size of approximately 14 ± 1 nm (Fig. 8a, b).

HR-TEM indicated the amorphous crystal structure of the Gd NPs. In addition, EDX confirmed the presence of the gadolinium spectra (Fig. 8b, d).

The XRD-spectra of the synthesised Gd NPs is shown in Fig. 9. Based on the reference, JCPDS No 86–2477 [23], the peaks appear at 2 theta 29.87°, 31.76 °, 39.60°, 43.56 °, 46.03°, and 57.79° corresponding to (222), (123), (332), (134), (440) and (622) of the gadolinium cubic phase planar, respectively [15,24].
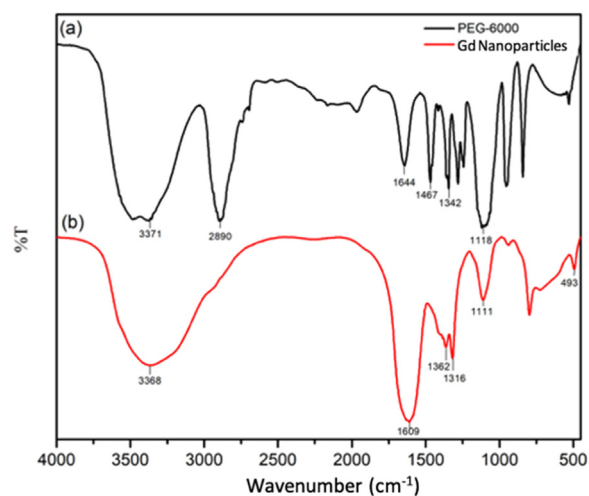
3.9. FTIR characterisation of the Gd NPs

Fig. 10 shows the spectra of (a) PEG-6000 and (b) Gd NPs synthesised under the optimal conditions. Fig. 10a shows characteristic vibration bands of PEG at 3371 and 1644 cm^{-1} (–O–H stretching and bending), 2890, 1467, and 1342 cm^{-1} (–C–H stretching and bending), and 1118 cm^{-1} (C–O–C stretching). Furthermore, some strong vibrational bands of PEG at 2890 and 1467 cm^{-1} represented stretching and bending vibrations of –CH$_2$CH$_2$– symmetric, indicating the presence of saturated carbon –(CH$_2$CH$_2$)n–. In Fig. 10b, the intensity of the vibrational bands related to aliphatic C–H stretching and bending was significantly reduced, suggesting that PEG molecules were present at low intensity in

Table 4

Comparison of Gd NPs synthesised via various methods.

Preparation method	Template/ modification	Size (nm)	Reference
Sol-gel	EG[1]	38, 49, 60, and 74	[1]
Polyol	DEG[2] and TEG[3]	18–30	[11]
Solvothermal	PEG-1000	80	[13]
Thermal decomposition	PEG	178	[14]
Pulsed Laser Ablation	PEG	15, 11, and 6	[15]
Hydrothermal	Dextrose	A few (nm)	[28]
Hydrothermal	PEG (with boric acid)	20	[29]
Hydrothermal[4]	PEG	14	This study

[1] Ethylene glycol.

[2] Diethylene glycol.

[3] Triethylene glycol.

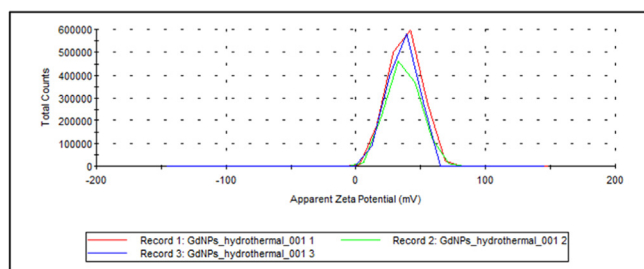[4] Combination with experimental design (RSM-BBD).

Fig. 11. Zeta potential characterisation of Gd NPs.

the Gd NPs. A vibrational band at 493 cm^{-1} was also observed indicative of Gd–O vibration. This is consistent with Ref. [25], where IR vibrational bands were detected below 500 cm^{-1} and were associated with Gd–O vibrations.

3.10. Characterisation of Gd NPs with the zeta potential

The zeta potential values indicate the potential stability of the colloidal system. When particles in suspension had high negative or positive zeta potentials, this shows a tendency for electrostatic repulsion amongst particles, thereby preventing flocculation (the aggregation of small colloids into larger ones). According to Ref. [26], zeta potential values below −30 mV and above +30 mV have sufficient repulsive forces to achieve better colloidal stability. Low zeta potential values could cause particles to aggregate and flocculate due to van der Waals forces, leading to their physical instability.

Based on Fig. 11, the particle charge analysis (zeta potential) in the range of −200 mV to 200 mV indicates an average zeta potential value of +36.7±0.802 mV. This parameter shows the level of electrostatic repulsion amongst the charged particles and was moderately stable. However, other factors, such as particle size, distribution, and morphology also influence the stability of the nanoparticles [27]. As observed in the SEM micrograph, nanoparticle agglomeration still tended to occur.

4. Conclusion

In conclusion, the optimal conditions for hydrothermal synthesis of spherical Gd NPs less than 20 nm were successfully determined by RSM-BBD (Table 4). The smallest size of Gd NPs was achieved by varying three crucial parameters, such as the mass of Gd_2O_3 (g), the synthesis temperature (°C) and time (h) based on Minitab 18 software. From the characterisation results of synthesised GdNPs, their zeta potential also indicated good stability of the Gd NPs due to the distributed PEG molecules. However, FTIR revealed the low intensity of PEG molecules on the Gd NPs. Therefore, further PEG modification must be performed

as an alternative startegy to utilise the Gd NPs for biomedical applications.

Declaration of Competing Interest

The authors declare that they have no known competing financial interests or personal relationships that could have appeared to influence the work reported in this paper.

References

[1] Whba F, Mohamed F, Md Rosli NRA, Abdul Rahman I, Idris MI. The crystalline structure of gadolinium oxide nanoparticles (Gd2O3-NPs) synthesized at different temperatures via X-ray diffraction (XRD) technique. Radiat Phys Chem 2021;179. doi:10.1016/j.radphyschem.2020.109212.

[2] Fatima A, Ahmad MW, Al Saidi AKA, Choudhury A, Chang Y, Lee GH. Recent advances in gadolinium-based contrast agents for bioimaging applications. Nanomaterials 2021;11. doi:10.3390/nano11092449.

[3] Fauzia RP, Denkova AG, Djanashvili K. Potential of MRI in radiotherapy mediated by small conjugates and nanosystems. Inorganics 2019;7 Basel. doi:10.3390/inorganics7050059.

[4] Li H, Zeng Y, Zhang H, Gu Z, Gong Q, Luo K. Functional gadolinium-based nanoscale systems for cancer theranostics. J Controll Release 2021;329:482–512. doi:10.1016/j.jconrel.2020.08.064.

[5] Vergauwen E, Vanbinst AM, Brussaard C, Janssens P, De Clerck D, Van Lint M, et al. Central nervous system gadolinium accumulation in patients undergoing periodical contrast MRI screening for hereditary tumor syndromes. Hered Cancer Clin Pract 2018;16:2. doi:10.1186/s13053-017-0084-7.

[6] Zhang B, Liang L, Chen W, Liang C, Zhang S. An updated study to determine association between gadolinium-based contrast agents and nephrogenic systemic fibrosis. PLOS One 2015;10:e0129720.

[7] Fauzia RP, Mutalib A, Soedjanaatmadja RUMS, Bahti HH, Anggraeni A, Gunawan AH, et al. Synthesis and characterization of gadolinium diethylenetriamine pentaacetate-folate. Procedia Chem 2015;17:139–46. doi:10.1016/j.proche.2015.12.128.

[8] Azooz EA, Ridha RK, Abdulridha HA. The fundamentals and recent applications of micellar system extraction for nanoparticles and bioactive molecules: a review. Nano Biomed Eng 2021;13:264–78 10.5101/nbe.v13i3. p264-278.

[9] Kaswer A., Al-Toriahi M., Adnan Azooz E., Abbas E., Al-Mulla J., Al-Toriahi K.M., et al. Metal nanoparticles and nano-filters for the disposal of hospital waste: a review 2023. doi:10.26599/NBE.2023.9290017.

[10] Ealias AM, Saravanakumar MP. A review on the classification, characterisation, synthesis of nanoparticles and their application. In: Proceedings of the IOP conference series: materials science and engineering, 263. Institute of Physics Publishing; 2017. doi:10.1088/1757-899X/263/3/032019.

[11] Setiawan H, Triyatna F, Nurmanjaya A, Subechi M, Sarwono DA, Billah AA, et al. Synthesis and characterization of gadolinium nanoparticles using polyol method as a candidate for MRI contrast agent. In: Proceedings of the journal of physics: conference series, 2193. Institute of Physics; 2022. doi:10.1088/1742-6596/2193/1/012010.

[12] Junejo Y, Baykal A, Sözeri H. Simple hydrothermal synthesis of Fe_3O_4-PEG nanocomposite. Cent Eur J Chem 2013;11:1527–32. doi:10.2478/s11532-013-0281-9.

[13] Dougherty A, Nasution ELY, Iskandar F, Dougherty G. Facile solvothermal synthesis and functionalization of polyethylene glycol-coated paramagnetic $Gd_2(CO_3)_3$ particles and corresponding Gd_2O_3 nanoparticles for use as MRI contrast agents. J Sci Adv Mater Devices 2019;4:72–9. doi:10.1016/j.jsamd.2018.12.005.

[14] Ahab A, Rohman F, Iskandar F, Haryanto F, Arif I. A simple straightforward thermal decomposition synthesis of PEG-covered Gd_2O_3 (Gd_2O_3@PEG) nanoparticles. Adv Powder Technol 2016;27:1800–5. doi:10.1016/j.apt.2016.06.012.

[15] Dougherty A, Harper C, Iskandar F, Arif I, Dougherty G. *In situ* functionalization of gadolinium oxide nanoparticles with polyethylene glycol (PEG) by pulsed laser ablation in a liquid medium (PLAL). J Sci Adv Mater Devices 2018;3:419–27. doi:10.1016/j.jsamd.2018.08.003.

[16] Selvalakshmi T, Bose AC. Optical study on gadolinium oxide nanoparticles synthesized by hydrothermal method. Adv Mat Res 2012;585:105–9. doi:10.4028/www.scientific.net/AMR.585.105.

[17] Permana A, Hardi Purba H, Hasibuan S. Design of experiment (DOE) analysis with response surface method (RSM) to optimize the electroplating parameter. ComTech Comput Math Eng Appl 2021;12:99–109. doi:10.21512/comtech.v12i2.6998.

[18] Wyantuti S, Pratomo U, Manullang LA, Hendrati D, Hartati YW, Bahti HH. Development of differential pulse voltammetric method for determining samarium (III) through electroanalytical study of the metal ion in acetonitrile using Box–Behnken design. Heliyon 2021;7. doi:10.1016/j.heliyon.2021.e06602.

[19] Wu L, Yick KL, Ng SP, Yip J. Application of the Box-Behnken design to the optimization of process parameters in foam cup molding. Expert Syst Appl 2012;39:8059–65. doi:10.1016/j.eswa.2012.01.137.

[20] Shi L, Zhang J, Zhao M, Tang S, Cheng X, Zhang W, et al. Effects of polyethylene glycol on the surface of nanoparticles for targeted drug delivery. Nanoscale 2021;13:10748–64. doi:10.1039/d1nr02065j.

[21] Wyantuti S, Iskandar J, Putri Fauzia R, Bahti HH. Optimization of hydrothermal synthesis of dysprosium oxide nanoparticles-attached-polyethyleneglycol template using response surface methodology-Box-Behnken. Nano Hybrids Compos 2023;40:13–18. doi:10.4028/p-6ytPC9.

[22] 4 - A systematic methodology for Design of Experiments Antony J, Antony J. Design of experiments for engineers and scientists Oxford: Butterworth-Heinemann; 2003. p. 29–43. doi:10.1016/B978-075064709-0/50005-3.

[23] Madhuri SN, Hemalatha KS, Rukmani K. Preparation and investigation of suitability of gadolinium oxide nanoparticle doped polyvinyl alcohol films for optoelectronic applications. J Mater Sci Mater Electron 2019. doi:10.1007/s10854-019-01237-9.

[24] Kumar A, Sarkar T, Solanki PR. Amine functionalized gadolinium oxide nanoparticles-based electrochemical immunosensor for cholera. Biosensors 2023;13 Basel. doi:10.3390/bios13020177.

[25] Chaudhary S, Kumar S, Kumar S, Chaudhary GR, Mehta SK, Umar A. Ethylene glycol functionalized gadolinium oxide nanoparticles as a potential electrochemical sensing platform for hydrazine and p-nitrophenol. Coatings 2019;9. doi:10.3390/coatings9100633.

[26] Joseph E, Singhvi G, Grumezescu AM. Chapter 4 - Multifunctional nanocrystals for cancer therapy: a potential nanocarrier. In: Nanomaterials for drug delivery and therapy. William Andrew Publishing; 2019. p. 91–116. doi:10.1016/B978-0-12-816505-8.00007-2.

[27] Mutia Windy Y., Natasya Dilla K., Claudia J., Rakhman Hakim A. Characterization and formulation of nanoparticles extract of bundung plant (Actinoscirpus Grossus) with variations in concentration of chitosan and Na-TPP bases using the ionic gelation method n.d. 2023. 10.33084/jsm.vxix.xxx.

[28] Babić-Stojić B, Jokanović V, Milivojević D, Požek M, Jagličić Z, Makovec D, et al. Gd2O3 nanoparticles stabilized by hydrothermally modified dextrose for positive contrast magnetic resonance imaging. J Magn Magn Mater 2016;403:118–26. doi:10.1016/j.jmmm.2015.11.075.

[29] Mikami K, Kanetaka H, Furuya M, Yokota K, Saijo Y, Yokoi T, et al. Hydrothermal synthesis and preliminary cytotoxicity assessment of gadolinium borate nanoparticles for neutron capture therapy. J Nanopart Res 2021;23. doi:10.1007/s11051-021-05311-4.